

Phase Separation in Doped Mott Insulators

Chuck-Hou Yee*

*Department of Physics and Astronomy, Rutgers, The State University of New Jersey,
Piscataway, New Jersey 08854, USA*

Leon Balents

*Kavli Institute for Theoretical Physics, University of California, Santa Barbara, California 93106, USA
(Received 3 July 2014; published 15 April 2015)*

Motivated by the commonplace observation of Mott insulators away from integer filling, we construct a simple thermodynamic argument for phase separation in first-order doping-driven Mott transitions. We show how to compute the critical dopings required to drive the Mott transition using electronic structure calculations for the titanate family of perovskites, finding good agreement with experiment. The theory predicts that the transition is percolative and should exhibit Coulomb frustration.

DOI: [10.1103/PhysRevX.5.021007](https://doi.org/10.1103/PhysRevX.5.021007)

Subject Areas: Condensed Matter Physics,
Strongly Correlated Materials

I. INTRODUCTION

The Mott transition is a pervasive and complex phenomena, observed in many correlated oxide systems [1]. It comes in two varieties: the bandwidth-controlled transition at half-filling, tuned by the ratio of the on-site Coulomb repulsion U and bandwidth W , and the filling-controlled transition, tuned by electron doping x away from half-filling. Theoretically, Mott insulators exist only at half-filling: With one electron per site, hoppings necessarily create empty and doubly occupied sites that are heavily penalized by U . Introducing a finite charge density allows carriers to move without incurring the on-site Coulomb cost, destroying the Mott insulator [2]. However, experiments in a wide variety of transition metal oxides show that the critical doping x_c needed to destroy insulating transport is not zero but rather a substantial fraction of unity [3], ranging from 0.1 in the nickelates [4] to 0.5 in the vanadates [5]. Systematic variations of x_c with bandwidths also show that it is an intrinsic quantity [6] and motivate the search for mechanisms independent of disorder or coupling to lattice vibrations for insulating behavior away from half-filling.

The scenario of doping a Mott insulator has been heavily studied using a variety of techniques [7–10]. For the classic case of a square lattice, basic issues such as whether the Mott transition is first [11–14] or second [15–18] order, the specific parameter regimes and underlying mechanisms of phase separation [19–24], and the structure of the

inhomogeneous phases [25–27] have been actively researched, with results dependent on the specific model considered and technique applied. We take a different approach: We assume the *bandwidth*-controlled Mott transition is first order and deduce its implications by constructing a simple thermodynamic description. We predict that the filling-controlled transition is first order as a consequence, implying that phase separation occurs and the critical doping scales as $x_c \sim \sqrt{U - U_c}$, where U_c defines the critical U for the bandwidth-controlled transition. Using the prototypical example of the rare-earth titanates, an experimentally [28,29] and theoretically [30–32] well-characterized family of Mott compounds, we show how to compute x_c within electronic structure calculations [33].

II. THERMODYNAMICS

We construct a theory of the Mott transition by connecting the bandwidth- and filling-controlled transitions. By assuming the former transition is first order (which covers the majority of cases observed in experiment), we can explicitly write down the energy densities $\epsilon = E/V$ for the metallic and insulating states since the two states must independently exist over a finite parameter range and cross at the first-order transition. We determine the phase boundary of the Mott transition in the μ - U plane (μ is the chemical potential) and compute the scaling of the critical doping x_c with U .

Consider a one-band Hubbard model on a generic lattice. The μ - U phase diagram generically consists of two regions: a Mott insulator occupying a finite range in μ at sufficiently large $U > U_c$ and a Fermi liquid (actually a superconductor or any other compressible phase including a possible non-Fermi liquid will suffice for the argument) everywhere else (Fig. 1). Expanding the grand-canonical energy densities

*chuckyee@physics.rutgers.edu

Published by the American Physical Society under the terms of the Creative Commons Attribution 3.0 License. Further distribution of this work must maintain attribution to the author(s) and the published article's title, journal citation, and DOI.

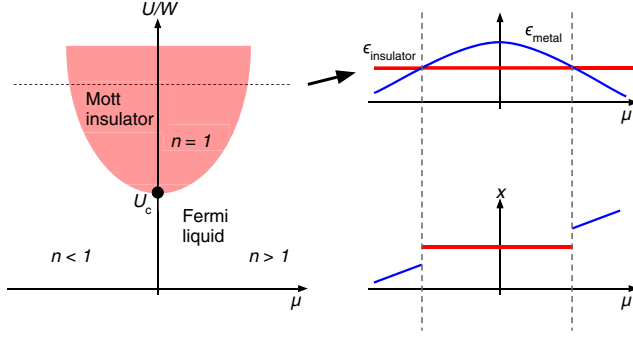


FIG. 1. The phase diagram for the Mott transition, plotted as a function of interaction strength U and chemical potential μ . The energy vs μ curve at constant U exhibits level crossings between the metallic and insulating states. The discontinuity in the derivative $x = -\partial\epsilon/\partial\mu$ implies thermodynamically forbidden densities where the system will phase separate into undoped $x = 0$ and critically doped $x = x_c$ patches.

of the metal and insulator to lowest order about the bandwidth-controlled transition point (dot labeled U_c in Fig. 1), we obtain

$$\epsilon_m(\mu, U) = \epsilon_0 + d_m \Delta U - \frac{1}{2} \kappa (\Delta \mu)^2, \quad (1)$$

$$\epsilon_i(\mu, U) = \epsilon_0 + d_i \Delta U. \quad (2)$$

Here, $\kappa = \partial x / \partial \mu$ is the electronic compressibility, where the doping $x = n - 1$ is defined relative to half-filling, and d_m and d_i are the per-site double occupancies $\langle n_{i\uparrow} n_{i\downarrow} \rangle$ in the metallic and insulating states. The chemical potential $\Delta \mu = \mu - \mu_{n=1}$ and Coulomb repulsion $\Delta U = U - U_c$ are measured relative to the bandwidth-controlled transition point.

Equating the two energies, we obtain the Mott phase boundary,

$$\Delta U = \frac{\Delta \mu^2}{2} \frac{\kappa}{d_m - d_i}. \quad (3)$$

Evaluating the metallic density $x = -\partial\epsilon_m/\partial\mu$ along the phase boundary, we obtain the critical doping

$$x_c = \sqrt{\Delta U \cdot 2\kappa(d_m - d_i)}. \quad (4)$$

Similar to the liquid-gas transition, thermodynamics forbids charge densities lying in the range $0 < |x| < x_c$. The system will phase separate if doped to lie within this regime [24].

We note that the filling-controlled transition is not doping in the conventional sense, where the insulator is connected to a metal formed by shifting μ into the bands lying adjacent to the spectral gap. Indeed, the smallness of $\Delta \mu$ for small ΔU implied by Eq. (3) dictates that the first-order transition occurs without the closing of the

single-particle gap, when ΔU is small. Rather, the Mott insulator transitions to a disconnected, lower-energy, metallic state [11].

III. PHASE SEPARATION

Thermodynamics forbids charge densities in the range $0 < |x| < x_c$, causing the system to phase separate into insulating regions with $x = 0$ and metallic regions with $x = x_c$ (shaded region in Fig. 2). The surface energy $E_{\text{surface}} \sim \sigma L^{d-1}$, where $\sigma > 0$ is the surface tension and L is the characteristic size of a metallic region, favors forming a single large puddle. However, the long-ranged part of the Coulomb interaction $E_{\text{Coul}} \sim x_c^2 L^{2d-1}$ penalizes macroscopic charge imbalances. Balancing the two gives domains of typical size $L \sim (\sigma/x_c^2)^{1/d}$. The actual spatial patterns formed depend on system-specific details such as dimensionality, anisotropy, and elastic forces [26].

Conducting transport does not coincide with the disappearance of phase separation at x_c and the formation of the homogeneous metallic state. Instead, when the volume fraction $x/x_c \sim \phi$ of the metallic puddles reaches the percolation limit, roughly $\phi_c \sim 1/3$ in three dimensions [34], conduction occurs across the system. Depending on the spatial patterns favored, we may expect anisotropic transport. Additionally, we predict an intermediate conducting magnetic state (AF-M in Fig. 2) since long-range order persists as long as the insulating regions percolate, up to a doping $x/x_c \sim 1 - \phi_c$. This intermediate state does not exist in two dimensions since $\phi_c \sim 1/2$, implying that the metallic and insulating states never simultaneously percolate.

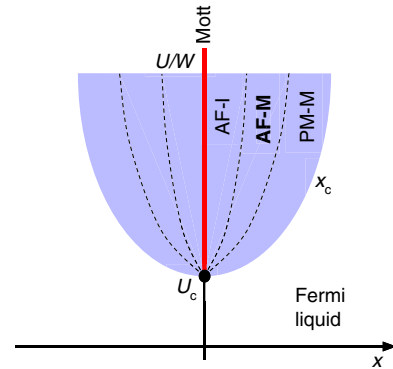


FIG. 2. Generic Mott phase diagram for a three-dimensional (3D) system plotted in the U vs x plane. Beginning at the pure Mott insulating state at zero doping $x = 0$, we progress through three phase-separated states (shaded) to arrive at a uniform Fermi liquid. The three phase-separated states have distinct magnetic (AF or PM) and transport (M or I) signatures. Since the percolation threshold $\phi_c^{3D} \sim 1/3$, we expect an intermediate phase (AF-M, bolded text) where metallic conductivity coexists with magnetic order. This intermediate phase is absent in 2D since $\phi_c^{2D} \sim 1/2$, so the metal and insulator are never simultaneously percolated.

IV. AB INITIO MODELING

The rare earth titanates $RTiO_3$ are an ideal system to investigate the Mott transition [28,29]. Varying the ionic radius of the rare earth R tunes the correlation strength, while rare earth vacancies [35] or Ca substitution [6] tune the Ti valence from d^1 to d^0 . The interplay between structure, transport, and magnetism is well characterized. Critical dopings, determined via transport, range from 0.05 in $LaTiO_3$ to 0.35 in $YTiO_3$, and the predicted intermediate metallic antiferromagnetic state has been observed [6], although the claim is not without controversy [36]. Careful bulk measurements suggest signatures of phase separation [37,38]. However, these prior studies suffer from chemical disorder due to the divalent substitution used to obtain filling control, so recent synthesis of high-quality electrostatically doped heterostructures opens the possibility of filling control without cation disorder [39].

To apply our theory to the titanates, we perform electronic structure calculations using the combination of density functional theory and dynamical mean-field theory [33] with the implementation described in Ref. [40]. We used $U = 9.0$ eV and $J = 0.8$ eV for the strength of the Coulomb repulsion on the Ti t_{2g} orbitals, and $E_{dc} = U(n_d - 1/2) - J(n_d - 1)/2$ with $n_d = 1.0$ as the standard double-counting energy. The empty e_g orbitals do not require correlations for their correct description. We include all the valence states, notably the oxygen $2p$ states in the hybridization window. We use $T = 100$ K, well below the Mott transition temperature at half-filling. The value for U was determined by requiring the calculated gap of the end-member $LaTiO_3$ to match the experimentally determined value, reported to be in the range 20 meV to 0.2 eV [41]. Once fixed, these parameters were used for the entire $RTiO_3$ family. To capture correlations in the $4f$ shells of the compounds with partially filled rare earth ions, we applied the atomic self-energy

$$\Sigma_f(i\omega_n) = \Sigma_0 + \frac{U_f^2 p(1-p)}{i\omega_n + \mu - U_f(p - 1/2)}, \quad (5)$$

with the static shift $\Sigma_0 = -U_f(p - 1/2) - \epsilon_f$. Here, $U_f = 10$ eV is the Hartree term on the f shell, ϵ_f is the center of mass of the f density of states, and p is the filling fraction (e.g., $3/14$ for $NdTiO_3$). Since the chemical potential is the independent variable in the scans needed to compute the n vs μ curves, we do not update the charge density, as this would require self-consistent adjustment of the nuclear charges. To obtain spectral quantities, we analytically continued the $3d$ self-energy Σ onto the real axis by applying the maximum entropy method to the effective Green's function $G = 1/[i\omega_n - E - \Sigma(i\omega_n)]$.

Shown in Fig. 3 is the density of states for the end compounds $LaTiO_3$ and $YTiO_3$. The contraction of the cation ionic radii from La to Y enhances the octahedral

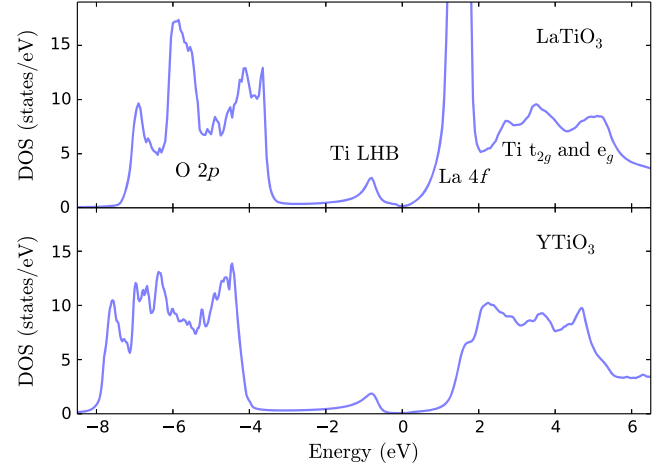


FIG. 3. Density of states for end members $LaTiO_3$ and $YTiO_3$ of the $RTiO_3$ series computed using DFT + DMFT. The reduction of bandwidth in $YTiO_3$ enhances the relative strength of correlations and produces a larger spectral gap. We emphasize that a single set of Coulomb parameters was used for both simulations, and the differences are driven purely by chemistry.

distortions, reducing the bandwidth of $YTiO_3$ relative to $LaTiO_3$ (observed within DFT). The reduction places the $YTiO_3$ deeper inside the Mott insulating state, which is reflected in the increased spectral gap of nearly 2 eV. The salient features—the location of the lower Hubbard band and oxygen $2p$ binding energies—agree well with photoemission [42,43].

We explicitly determine the critical doping x_c of the titanates by monitoring the charge density as we lower the chemical potential to hole dope the Mott insulator (Fig. 4). The critical doping, as given by the discontinuity between the insulator and Fermi liquid, increases monotonically

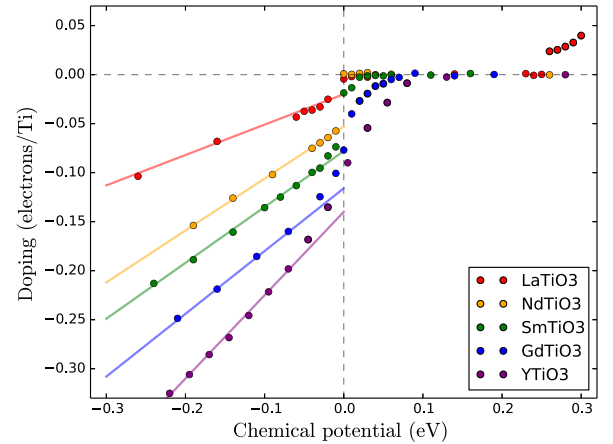


FIG. 4. Doping as a function of chemical potential near the hole-doped Mott transition, computed with DFT + DMFT for representative members of the $RTiO_3$ family. The size of the density discontinuity (the critical doping x_c) increases as we progress away from the largest rare earth La. The lines are guides to the eye. The electron-doped transition can be seen for $LaTiO_3$ in the upper right.

TABLE I. For representative titanates, we tabulate the electronic compressibility per Ti atom $\kappa = \partial n / \partial \mu$, Hartree component of the potential energy $d_{m,i} = \langle N(N-1)/2 \rangle$ in the metallic and insulating states, and the critical Coulomb strengths U_c . Using $\Delta U = U - U_c$ where $U = 9$ eV in our calculations, and Eq. (4), we compute the critical doping x_c .

Compound	κ (e/eV)	d_m	d_i	U_c (eV)	x_c
LaTiO ₃	0.20	0.15	0.13	8.8	4%
SmTiO ₃	0.22	0.22	0.19	6.0	20%
YTiO ₃	0.28	0.23	0.20	4.7	27%

from about 2% for La to about 15% for Y, corroborating our expectation that correlations increase x_c . We note that the small contribution to the compressibility due to the partially filled 4*f* shells for the intermediate rare earths has been subtracted out to give a flat n vs μ curve in the Mott-insulating regime. We do not observe a jump in GdTiO₃ and YTiO₃ because the Mott critical endpoint drops below the simulation temperature of $T = 100$ K, as observed experimentally [6], so we roughly extract x_c by pinpointing the location of steepest slope in the n vs μ curve. The critical dopings are smaller than experiment by a factor of 2, which we attribute to the effect of the strong chemical disorder required for doping, as well as polaron formation, which is known to drive the finite- T Mott transition more strongly first order [44].

As a consistency check, we also determine x_c for representative compounds using Eq. (4), which is valid near the bandwidth-controlled transition point. First, we determined the critical Coulomb strengths U_c for the bandwidth-controlled transition, which decrease from LaTiO₃ to YTiO₃ as expected. The charge compressibility was obtained by scanning n vs μ at U_c . To obtain the “double occupancy” of the metallic and insulating solutions, we note that in multiband models, the Coulomb U couples to the generalization of the on-site double occupancies—the Hartree component of the potential energy— $N_i(N_i - 1)/2$, where N_i runs from 0 to 10 within the 3*d* manifold. The extracted parameters are shown in Table. I. Again, x_c increases as we progress from the least- to the most-correlated compounds and roughly agree with the values inferred from the n vs μ curves, even for YTiO₃, which is quite far from the bandwidth-controlled transition.

V. SUMMARY

We have outlined a theory for the first-order filling-controlled Mott transition, which predicts intrinsic electronic phase separation when a Mott insulator is doped away from half-filling, and we demonstrated explicitly how to calculate the critical doping x_c in electronic structure calculations for a family of titanates. The thermodynamic signatures of this pervasive phase separation have been observed in many other correlated systems [1], as well as directly using near-field optics on VO₂ [45] and STM in

the cuprates [46]. The key tasks to enhance the quantitative agreement between theory and experiment involve (a) including disorder and polarons into theoretical calculations and (b) designing cleaner experimental systems where chemical disorder can be reduced, e.g., through modulation-doped samples or oxide heterostructures. The accessibility of thin films to spatially resolved probes (STM, spatially resolved optics) is especially advantageous as they would allow direct visualization of the phase-separated region.

ACKNOWLEDGMENTS

This work was supported by the MRSEC Program of the National Science Foundation under Grant No. DMR 1121053. We benefitted from facilities of the KITP, funded by NSF Grant No. PHY-11-25915.

- [1] M. Imada, A. Fujimori, and Y. Tokura, *Metal-insulator transitions*, *Rev. Mod. Phys.* **70**, 1039 (1998).
- [2] P. Fazekas, *Lecture Notes on Electron Correlation and Magnetism*, Series in Modern Condensed Matter Physics, Vol. 5 (World Scientific, Singapore, 1999).
- [3] A. Fujimori, *Electronic structure of metallic oxides: Band-gap closure and valence control*, *J. Phys. Chem. Solids* **53**, 1595 (1992).
- [4] P.-H. Xiang, S. Asanuma, H. Yamada, I. H. Inoue, H. Akoh, and A. Sawa, *Room temperature Mott metal-insulator transition and its systematic control in Sm_{1-x}Ca_xNiO₃ thin films*, *Appl. Phys. Lett.* **97**, 032114 (2010).
- [5] A. A. Belik, R. V. Shpanchenko, and E. Takayama-Muromachi, *Carrier-doping metal-insulator transition in solid solutions of CdVO₃ – YVO₃*, *J. Magn. Magn. Mater.* **310**, e240 (2007).
- [6] T. Katsufuji, Y. Taguchi, and Y. Tokura, *Transport and magnetic properties of a Mott-Hubbard system whose bandwidth and band filling are both controllable: R_{1-x}Ca_xTiO_{3+y/2}*, *Phys. Rev. B* **56**, 10145 (1997).
- [7] H. Kajueter, G. Kotliar, and G. Moeller, *Doped Mott insulator: Results from mean-field theory*, *Phys. Rev. B* **53**, 16214 (1996).
- [8] P. A. Lee, N. Nagaosa, and X.-G. Wen, *Doping a Mott insulator: Physics of high-temperature superconductivity*, *Rev. Mod. Phys.* **78**, 17 (2006).
- [9] G. Kotliar and A. E. Ruckenstein, *New Functional Integral Approach to Strongly Correlated Fermi Systems: The Gutzwiller Approximation as a Saddle Point*, *Phys. Rev. Lett.* **57**, 1362 (1986).
- [10] S. Onoda and M. Imada, *Filling-control metal-insulator transition in the Hubbard model studied by the operator projection method*, *J. Phys. Soc. Jpn.* **70**, 3398 (2001).
- [11] M. Balzer, B. Kyung, D. Sénéchal, A.-M. S. Tremblay, and M. Pothoff, *First-order Mott transition at zero temperature in two dimensions: Variational plaquette study*, *Europhys. Lett.* **85**, 17002 (2009).
- [12] G. Sordi, K. Haule, and A.-M. S. Tremblay, *Finite Doping Signatures of the Mott Transition in the Two-Dimensional Hubbard Model*, *Phys. Rev. Lett.* **104**, 226402 (2010).

- [13] G. Sordi, K. Haule, and A.-M. S. Tremblay, *Mott physics and first-order transition between two metals in the normal-state phase diagram of the two-dimensional Hubbard model*, *Phys. Rev. B* **84**, 075161 (2011).
- [14] T. Misawa and M. Imada, *Origin of high- T_c superconductivity in doped Hubbard models and their extensions: Roles of uniform charge fluctuations*, *Phys. Rev. B* **90**, 115137 (2014).
- [15] N. Furukawa and M. Imada, *Two-dimensional Hubbard model—metal insulator transition studied by Monte Carlo calculation—*, *J. Phys. Soc. Jpn.* **61**, 3331 (1992).
- [16] A. Georges, G. Kotliar, W. Krauth, and M. J. Rozenberg, *Dynamical mean-field theory of strongly correlated fermion systems and the limit of infinite dimensions*, *Rev. Mod. Phys.* **68**, 13 (1996).
- [17] P. Werner and A. Millis, *Doping-driven Mott transition in the one-band Hubbard model*, *Phys. Rev. B* **75**, 085108 (2007).
- [18] E. Gull, M. Ferrero, O. Parcollet, A. Georges, and A. J. Millis, *Momentum-space anisotropy and pseudogaps: A comparative cluster dynamical mean-field analysis of the doping-driven metal-insulator transition in the two-dimensional Hubbard model*, *Phys. Rev. B* **82**, 155101 (2010).
- [19] P. Visscher, *Phase separation instability in the Hubbard model*, *Phys. Rev. B* **10**, 943 (1974).
- [20] V. Emery, S. Kivelson, and H. Lin, *Phase Separation in the t - J Model*, *Phys. Rev. Lett.* **64**, 475 (1990).
- [21] L. Gehlhoff, *Phase separation in the one-band Hubbard model*, *J. Phys. Condens. Matter* **8**, 2851 (1996).
- [22] W. Putikka and M. Luchini, *Limits on phase separation for two-dimensional strongly correlated electrons*, *Phys. Rev. B* **62**, 1684 (2000).
- [23] S. White and D. Scalapino, *Phase separation and stripe formation in the two-dimensional t - J model: A comparison of numerical results*, *Phys. Rev. B* **61**, 6320 (2000).
- [24] D. Galanakis, E. Khatami, K. Mikelsons, A. Macridin, J. Moreno, D. A. Browne, and M. Jarrell, *Quantum criticality and incipient phase separation in the thermodynamic properties of the Hubbard model*, *Phil. Trans. R. Soc. A* **369**, 1670 (2011).
- [25] B. Spivak and S. A. Kivelson, *Transport in two dimensional electronic micro-emulsions*, *Ann. Phys. (Amsterdam)* **321**, 2071 (2006).
- [26] C. Ortix, J. Lorenzana, and C. Di Castro, *Universality classes for Coulomb frustrated phase separation*, *Physica B (Amsterdam)* **404**, 499 (2009).
- [27] A. Giuliani, J. L. Lebowitz, and E. H. Lieb, *Checkerboards, stripes, and corner energies in spin models with competing interactions*, *Phys. Rev. B* **84**, 064205 (2011).
- [28] J. Greedan, *The rare earth-titanium (III) perovskite oxides—An isostructural series with a remarkable variation in physical properties*, *J. Less Common Met.* **111**, 335 (1985).
- [29] M. Mochizuki and M. Imada, *Orbital physics in the perovskite Ti oxides*, *New J. Phys.* **6**, 154 (2004).
- [30] L. Craco, M. Laad, S. Leon, and E. Müller-Hartmann, *Insulator-metal transition in the doped $3d^1$ transition metal oxide LaTiO_3* , *Phys. Rev. B* **70**, 195116 (2004).
- [31] E. Pavarini, S. Biermann, A. Poteryaev, A. Lichtenstein, A. Georges, and O. Andersen, *Mott Transition and Suppression of Orbital Fluctuations in Orthorhombic $3d^1$ Perovskites*, *Phys. Rev. Lett.* **92**, 176403 (2004).
- [32] A. Liebsch, *Doping-driven Mott transition in $\text{La}_{1-x}\text{Sr}_x\text{TiO}_3$ via simultaneous electron and hole doping of t_{2g} subbands as predicted by LDA + DMFT calculations*, *Phys. Rev. B* **77**, 115115 (2008).
- [33] G. Kotliar, S. Savrasov, K. Haule, V. Oudovenko, O. Parcollet, and C. Marianetti, *Electronic structure calculations with dynamical mean-field theory*, *Rev. Mod. Phys.* **78**, 865 (2006).
- [34] J. Essam, *Percolation theory*, *Rep. Prog. Phys.* **43**, 833 (1980).
- [35] A. Sefat, J. Greedan, and L. Cranswick, *Effect of hole doping on the magnetic properties of the Mott-Hubbard antiferromagnetic insulator $\text{Nd}_{1-x}\text{TiO}_3$* , *Phys. Rev. B* **74**, 104418 (2006).
- [36] A. Sefat, J. Greedan, G. Luke, M. Niéwcza, J. Garrett, H. Dabkowska, and A. Dabkowski, *Anderson-Mott transition induced by hole doping in $\text{Nd}_{1-x}\text{TiO}_3$* , *Phys. Rev. B* **74**, 104419 (2006).
- [37] C. Hays, J.-S. Zhou, J. Markert, and J. Goodenough, *Electronic transition in $\text{La}_{1-x}\text{Sr}_x\text{TiO}_3$* , *Phys. Rev. B* **60**, 10367 (1999).
- [38] H. Zhou and J. Goodenough, *Coexistence of two electronic phases in $\text{LaTiO}_{3+\delta}$ ($0.01 \leq \delta \leq 0.12$) and their evolution with δ* , *Phys. Rev. B* **71**, 165119 (2005).
- [39] P. Moetakef, T. A. Cain, D. G. Ouellette, J. Y. Zhang, D. O. Klenov, A. Janotti, C. G. Van de Walle, S. Rajan, S. J. Allen, and S. Stemmer, *Electrostatic carrier doping of $\text{GdTiO}_3/\text{SrTiO}_3$ interfaces*, *Appl. Phys. Lett.* **99**, 232116 (2011).
- [40] K. Haule, C.-H. Yee, and K. Kim, *Dynamical mean-field theory within the full-potential methods: Electronic structure of CeIrIn_5 , CeCoIn_5 , and CeRhIn_5* , *Phys. Rev. B* **81**, 195107 (2010).
- [41] P. Lunkenheimer, T. Rudolf, J. Hemberger, A. Pimenov, S. Tachos, F. Lichtenberg, and A. Loidl, *Dielectric properties and dynamical conductivity of LaTiO_3 : From dc to optical frequencies*, *Phys. Rev. B* **68**, 245108 (2003).
- [42] A. Fujimori, I. Hase, M. Nakamura, H. Namatame, Y. Fujishima, Y. Tokura, M. Abbate, F. de Groot, M. Czyzyk, J. Fuggle, O. Strebel, F. Lopez, M. Domke, and G. Kaindl, *Doping-induced changes in the electronic structure of $\text{La}_x\text{Sr}_{1-x}\text{TiO}_3$: Limitation of the one-electron rigid-band model and the Hubbard model*, *Phys. Rev. B* **46**, 9841 (1992).
- [43] A. Fujimori, I. Hase, H. Namatame, Y. Fujishima, Y. Tokura, K. Takegahara, and F. M. F. de Groot, *Evolution of the Spectral Function in Mott-Hubbard Systems with d^1 Configuration*, *Phys. Rev. Lett.* **69**, 1796 (1992).
- [44] M. Capone, G. Sangiovanni, C. Castellani, C. Di Castro, and M. Grilli, *Phase Separation Close to the Density-Driven Mott Transition in the Hubbard-Holstein Model*, *Phys. Rev. Lett.* **92**, 106401 (2004).
- [45] M. M. Qazilbash, M. Brehm, B.-G. Chae, P.-C. Ho, G. O. Andreev, B.-J. Kim, S. J. Yun, A. V. Balatsky, M. B. Maple, F. Keilmann, H.-T. Kim, and D. N. Basov, *Mott transition in VO_2 revealed by infrared spectroscopy and nano-imaging*, *Science* **318**, 1750 (2007).
- [46] Y. Kohsaka, T. Hanaguri, M. Azuma, M. Takano, J. C. Davis, and H. Takagi, *Visualization of the emergence of the pseudogap state and the evolution to superconductivity in a lightly hole-doped Mott insulator*, *Nat. Phys.* **8**, 534 (2012).